Corrosion Science 81 (2014) 54–64

Contents lists available at ScienceDirect

Corrosion Science

journal homepage: www.elsevier.com/locate/corsci

Three novel di-quaternary ammonium salts as corrosion inhibitors for API X65 steel pipeline in acidic solution. Part I: Experimental results

M.A. Hegazy [a,*], M. Abdallah [b,c], M.K. Awad [d], M. Rezk [c]

[a] Egyptian Petroleum Research Institute (EPRI), Nasr City, Cairo, Egypt
[b] Chemistry Department, Faculty of Applied Sciences, Umm Al-Qura University, Makkah, Saudi Arabia
[c] Chemistry Dept., Faculty of Science, Benha University, Benha, Egypt
[d] Chemistry Department, Theoretical Applied Chemistry Unit (TACU), Faculty of Science, Tanta University, Tanta, Egypt

ARTICLE INFO

Article history:
Received 21 October 2013
Accepted 9 December 2013
Available online 17 December 2013

Keywords:
A. Steel
B. EIS
B. Weight loss
B. Polarization
C. Acid inhibition
C. Interfaces

ABSTRACT

Three novel di-quaternary ammonium salts were synthesized, characterized, and tested as corrosion inhibitors for API X65 steel pipeline in 1 M HCl. The inhibition effect of the prepared compounds was studied by EIS, Tafel polarization and weight loss measurements. Polarization curves revealed that the prepared compounds act as mixed type inhibitors. It was found that the inhibition efficiency increased with increasing the compound concentration and decreasing the temperature and also is dependent on the molecular structures. Adsorption of the prepared compounds on API X65 steel pipeline surface is a physical adsorption and obeys the Langmuir's isotherm.

1. Introduction

Steel pipelines play an important role in transporting gases and liquids throughout the world [1]. Corrosion is a serious problem in steel pipelines because replacing, repairing, and maintaining them can be extremely expensive and time-consuming [2–6]. Acid solutions are generally used for removal of undesirable scales and rusts on steel surface in several industrial sectors and also widely applied to enhance oil/gas recovery through acidification in the oil and gas industry. These operations usually induce serious corrosion of equipment, tubes, and pipelines made of steel [7,8].

The use of inhibitors is one of the most convenient means for protection of steel corrosion in acidic solution as they can prevent metal from dissolution and consequently reduce the operation cost [9]. The existing data showed that the most of organic compounds which were used as corrosion inhibitors can be adsorbed on metal surface via heteroatom such as nitrogen, sulfur, oxygen and phosphorus, multiple bonds or aromatic rings and they block the active sites and accordingly, decreasing the corrosion rate [10,11]. The inhibition efficiency of organic inhibitors is mainly dependent on its affinity and compatibility to the metal surface [12]. Many efficient organic inhibitors have heteroatom and multiple bonds or aromatic rings in their structures. As a representative type of these organic inhibitors, quaternary ammonium salts have been demonstrated, to be highly effective in corrosion inhibition for different aggressive media, in our lab and by other previous research [13–15].

Surfactants are the molecules which composed of a polar hydrophilic group, the "head", and attached to a non-polar hydrophobic group, the "tail". In general, the inhibitory action of surfactant in aqueous solutions is due to a physical (electrostatic) adsorption or chemisorption of surfactant molecules onto the metallic surface, depending on the charge of the solid surface and the free energy change of transferring a hydrocarbon chain from water to the solid surface. The adsorption of a surfactant markedly changes the corrosion resisting property of a metal and for this reason, the study of the correlation between the adsorption and corrosion inhibition is of a considerable importance [16–19].

Gemini surfactant is a new generation of surfactants developed in recent years which consist of two hydrophilic and two hydrophobic groups and are separated by a spacer in a molecular structure. It has been demonstrated that this new surfactant exhibits properties superior to those of conventional surfactants, such as better solubility and greater effect in lowering the surface tension of water. During recent years, an increasing of interest has been focused on the investigation of the inhibition behavior of Gemini surfactants in various aggressive media [20–22].

* Corresponding author. Tel.: +20 1002653529; fax: +20 222747433.
E-mail address: mohamed_hgazy@yahoo.com (M.A. Hegazy).

0010-938X/$ - see front matter © 2013 Elsevier Ltd. All rights reserved.
http://dx.doi.org/10.1016/j.corsci.2013.12.010

In the present paper, three di-quaternary ammonium salts, namely N-(3-(2-(isopropyldimethylammonio)acetoxy)propyl)-N,N-dimethyldodecan-1-aminium chloride bromide (compound Q1), N-(3-(2-((2-hydroxyethyl)dimethylammonio)acetoxy)propyl)-N,N-dimethyldodecan-1-aminium chloride bromide (compound Q2) and N-(3-(2-(phenyldiethylammonio)acetoxy)propyl)-N,N-dimethyldodecan-1-aminium chloride bromide (compound Q3), were synthesized and characterized. The inhibition effect of these compounds for API X65 steel pipeline in 1 M HCl solution was evaluated by weight loss, potentiodynamic polarization and electrochemical impedance spectroscopy (EIS) measurements. The effect of the inhibitor concentration and temperature on the inhibition behavior was studied. Based on the experimental data, several thermodynamic and kinetic parameters were estimated. The adsorption mechanism of the prepared inhibitors onto API X65 steel pipeline surface in 1 M HCl was also discussed. Scanning electron microscope was used to examine the changes of surface morphology of the steel corroded in 1 M HCl with and without the addition of the inhibitors.

2. Materials and experimental techniques

2.1. Inhibitors

The three novel di-quaternary surfactants used in this study were synthesized in three steps as follow:

(i) Quaternization reaction [23] of 3-(dimethylamino)propan-1-ol (10.3 g, 0.1 mol) and 1-bromododecane (24.9 g, 0.1 mol) in ethanol at 70 °C for 48 h to produce N-(3-hydroxypropyl)-N,N-dimethyldodecan-1-aminium bromide. The mixture was allowed to cool-down. Then, the obtained mixture was further purified by diethyl ether and recrystallized by ethanol.

(ii) Esterification reaction [24] was carried out between the product obtained from the previous step (17.62 g, 0.5 mol) and 2-chloroacetic acid (4.72 g, 0.5 mol) in presence of xylene as a solvent and p-toluene sulfonic acid as a dehydrating agent to produce N-(3-(2-chloroacetoxy)propyl)-N,N-dimethyldodecan-1-aminium bromide. The reaction was completed when the concentration of the removed water is reached 0.5 M. The reaction mixture was distilled under a vacuum in order to remove the solvent completely.

(iii) Quaternization reaction [25] of the above product obtained from the previous step (4.29 g, 0.01 mol) with either N,N-dimethylpropan-2-amine (0.87 g, 0.01 mol), 3-(dimethylamino)propan-1-ol (1.03 g, 0.01 mol), or N,N-diethylaniline (1.49 g, 0.01 mol) in ethanol at 70 °C for 48 h to yield one of the following products, respectively:
   (1) N-(3-(2-(isopropyldimethylammonio)acetoxy)propyl)-N,N-dimethyldodecan-1-aminium chloride bromide (compound Q1).
   (2) N-(3-(2-((2-hydroxyethyl)dimethylammonio)acetoxy)propyl)-N,N-dimethyldodecan-1-aminium chloride bromide (compound Q2).
   (3) N-(3-(2-(phenyldiethylammonio)acetoxy)propyl)-N,N-dimethyldodecan-1-aminium chloride bromide (compound Q3).

The mixture was allowed to cool-down and then further purified by diethyl ether and recrystallized by ethanol.

Chemical structure of the synthesized inhibitors (Fig. 1) was confirmed by FTIR and ^{1}H NMR spectroscopy. FTIR analysis was

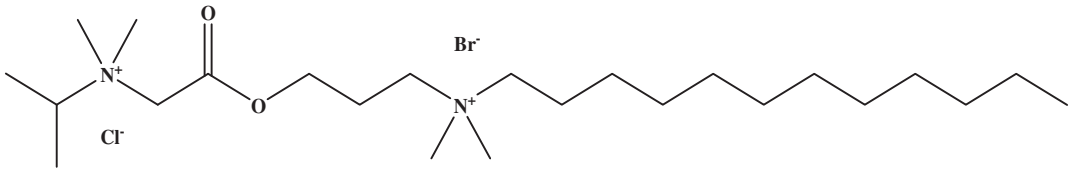

N-(3-(2-(isopropyldimethylammonio)acetoxy)propyl)-N,N-dimethyldodecan-1-aminium chloride bromide (compound Q1)

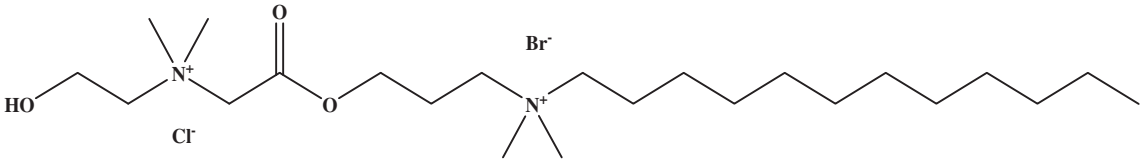

N-(3-(2-((2-hydroxyethyl)dimethylammonio)acetoxy)propyl)-N,N-dimethyldodecan-1-aminium chloride bromide (compound Q2)

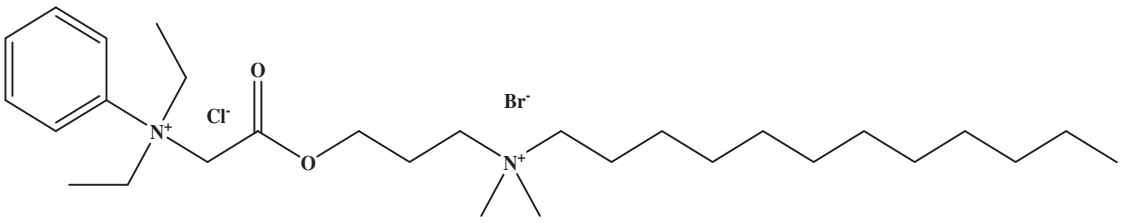

N-(3-(2-(phenyldiethylammonio)acetoxy)propyl)-N,N-dimethyldodecan-1-aminium chloride bromide (compound Q3)

Fig. 1. Chemical structure of the synthesized novel di-quaternary ammonium salts.

carried out using ATI Mattson infinity series TM, Bench top 961 controlled by Win First TM V2.01 software. ^{1}H NMR analysis was measured in DMSO-d_6 using Jeol ECA 500 MHZ NMR spectrometer.

2.2. Solutions

The aggressive solution, 1 M HCl, was prepared by diluting the analytical grade 37% HCl with distilled water. The concentration range of the synthesized inhibitors, used in corrosion measurements, was varied from 1×10^{-5} to 5×10^{-3} M.

2.3. Steel specimen

Tests were performed on a pipeline steel of the following chemical composition (wt.%): 0.28% C, 0.06% Ti, 1.40% Mn, 0.03% P, 0.03% S and the remainder is Fe. This material was made according to API 5L grade X65 specifications.

2.4. Weight loss measurements

A&D analytical balance, (Model: HR 200, readability: 0.1 mg and standard deviation: ±0.2 mg), was used for the gravimetric analysis. The API X65 steel pipeline sheets of 7 cm × 3 cm × 0.5 cm were abraded with a series of emery paper (grade 320–400–600–800–1000–1200) and then cleaned successively with distilled water, ethanol and acetone, and finally dried in dry air. After accurately weighting, the samples were immersed in 100 ml of 1 M HCl solution with and without the addition of different concentrations of di-quaternary surfactants at various temperatures. The temperature for weight loss measurements was controlled by water bath provided with thermostat control ±0.5 °C. The steel specimens were taken out after 24 h and then rinsed with distilled water twice and degreased with acetone. Then specimens were immersed in 1 M HCl solution for 10 s, (chemical method for cleaning rust products), rinsed twice with distilled water, ethanol, and acetone and finally dried in dry air and accurately weighted. The experiments were carried out in triplicates in order to give a good reproducibility and the average weight loss of three parallel API X65 steel pipeline sheets was obtained. All tests in this paper were done under aerated conditions.

2.5. Electrochemical measurements

The electrochemical experiments were carried out in a conventional three-electrode cell with a platinum counter electrode (CE) and a saturated calomel electrode (SCE) as a reference electrode. The working electrode (WE) was a rod of API X65 steel pipeline embedded in PVC holder using epoxy resin so that the flat surface was the only exposed surface in the electrode. The area of the working exposure surface was 0.7 cm^2. This area was abraded with emery paper (grade 320–400–600–800–1000–1200) on the test face, rinsed with distilled water, degreased with acetone and dried. Before measurement, the electrode was immersed in a test solution at open circuit potential (OCP) for 30 min. until a steady state was reached. All Electrochemical measurements were carried out using a VoltaLab 40 (PGZ301 & VoltaMaster 4) – (Radiometer Analytical-FRANCE) at 20 °C.

The potentiodynamic polarization measurements were obtained by changing the electrode potential automatically from −800 to −300 mV versus SCE with scan rate 2 mV s^{-1} at 20 °C. EIS measurements were carried out as described elsewhere [26]. A small alternating voltage perturbation (5 mV) was imposed on the cell over the frequency range from 100 kHz to 30 mHz at open circuit potential at 20 °C. Simulation of Nyquist diagrams with the suggested model was done by ZSimpWin program.

3. Results and discussion

3.1. Structure confirmation of the synthesized inhibitors

3.1.1. N-(3-hydroxypropyl)-N,N-dimethyldodecan-1-aminium bromide

3.1.1.1. FTIR spectroscopy. FTIR spectrum of N-(3-hydroxypropyl)-N,N-dimethyldodecan-1-aminium bromide showed the following absorption bands at 751.69 cm^{-1} ($(CH_2)_n$ rocking), 1373.10 cm^{-1} (CH_3 symmetric bending), 2859.14 cm^{-1} (CH symmetric stretching), 2937.80 cm^{-1} (CH asymmetric stretching), 1053.98 cm^{-1} ($C–N^+$) and 3389.87 cm^{-1} (OH). The FTIR spectrum confirmed the expected functional groups in the synthesized N-(3-hydroxypropyl)-N,N-dimethyldodecan-1-aminium bromide.

3.1.1.2. ^{1}H NMR spectroscopy. ^{1}H NMR (DMSO-d_6) spectrum (Fig. 2) of N-(3-hydroxypropyl)-N,N-dimethyldodecan-1-aminium bromide showed different bands at δ = 0.8105 ppm (t, 3H, $NCH_2CH_2(CH_2)_9C\underline{\mathbf{H}}_3$); δ = 1.2024 ppm (m, 18H, $NCH_2CH_2(C\underline{\mathbf{H}}_2)_9CH_3$); δ = 1.6007 ppm (m, 2H, $NCH_2C\underline{\mathbf{H}}_2(CH_2)_9CH_3$); δ = 3.2809 ppm (t, 2H, $NC\underline{\mathbf{H}}_2CH_2(CH_2)_9CH_3$); δ = 2.9809 ppm (s, 6H, $C\underline{\mathbf{H}}_3NC\underline{\mathbf{H}}_3$); δ = 3.3325 ppm (t, 2H, $NC\underline{\mathbf{H}}_2CH_2CH_2OH$); δ = 1.7689 ppm (t, 2H, $NCH_2C\underline{\mathbf{H}}_2CH_2OH$); δ = 3.4318 ppm (t, 2H, $NCH_2CH_2C\underline{\mathbf{H}}_2OH$); δ = 4.7600 ppm (s, 1H, $NCH_2CH_2CH_2O\underline{\mathbf{H}}$). The data of ^{1}H NMR spec-

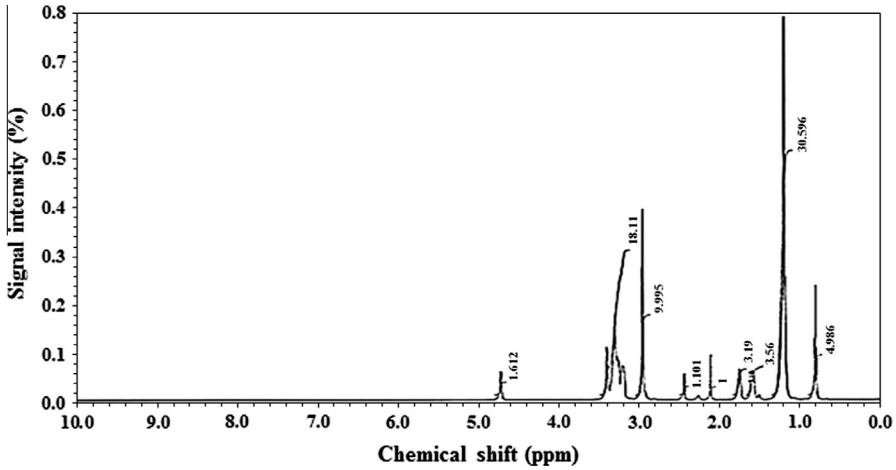

Fig. 2. ^{1}H NMR spectrum of N-(3-hydroxypropyl)-N,N-dimethyldodecan-1-aminium bromide.

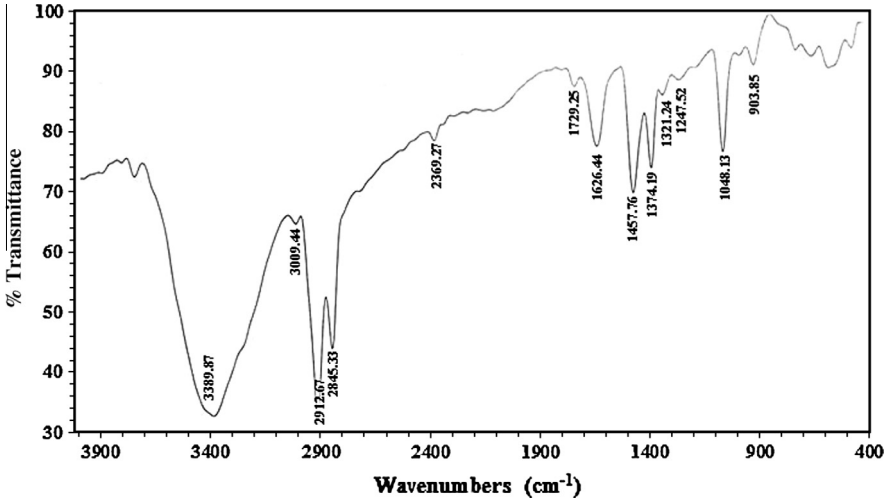

Fig. 3. FTIR spectrum of N-(3-(2-chloroacetoxy)propyl)-N,N-dimethyldodecan-1-aminium bromide.

tra confirmed the expected hydrogen proton distribution in the synthesized N-(3-hydroxypropyl)-N,N-dimethyldodecan-1-aminium bromide.

3.1.2. N-(3-(2-chloroacetoxy)propyl)-N,N-dimethyldodecan-1-aminium bromide

3.1.2.1. FTIR spectroscopy. FTIR spectrum of N-(3-(2-chloroacetoxy)propyl)-N,N-dimethyldodecan-1-aminium bromide (Fig. 3) showed the following absorption bands: 751.69 cm^{-1} ($(CH_2)_n$ rocking), 1374.19 cm^{-1} (CH_3 symmetric bending), 2845.33 cm^{-1} (CH symmetric stretching), 2912.67 cm^{-1} (CH asymmetric stretching), 1048.13 cm^{-1} ($C–N^+$). In addition to ester (COO) band appeared at 1729.25 cm^{-1} and disappearance of (OH) band at 3300 cm^{-1}. The FTIR spectrum confirmed the expected functional groups in the synthesized N-(3-(2-chloroacetoxy)propyl)-N,N-dimethyldodecan-1-aminium bromide.

3.1.2.2. ^1H NMR spectroscopy. ^1H NMR (DMSO-d_6) spectrum of N-(3-(2-chloroacetoxy)propyl)-N,N-dimethyldodecan-1-aminium bromide showed different bands at δ = 0.8396 ppm (t, 3H, $NCH_2CH_2(CH_2)_9C\underline{\mathbf{H}}_3$); δ = 1.2431 ppm (m, 18H, $NCH_2CH_2(C\underline{\mathbf{H}}_2)_9CH_3$); δ = 1.6909 ppm (m, 2H, $NCH_2C\underline{\mathbf{H}}_2(CH_2)_9CH_3$); δ = 3.2637 ppm (t, 2H, $NC\underline{\mathbf{H}}_2CH_2(CH_2)_9CH_3$); δ = 3.1857 ppm (s, 6H, $C\underline{\mathbf{H}}_3NC\underline{\mathbf{H}}_3$); δ = 3.3080 ppm (t, 2H, $NC\underline{\mathbf{H}}_2CH_2CH_2COOCH_2Cl$); δ = 2.0042 ppm (t, 2H, $NCH_2C\underline{\mathbf{H}}_2CH_2COOCH_2Cl$); δ = 4.1441 ppm (t, 2H, $NCH_2CH_2C\underline{\mathbf{H}}_2COOCH_2Cl$); δ = 5.3653 ppm (s, 1H, $NCH_2CH_2CH_2COOC\underline{\mathbf{H}}_2Cl$). The data of ^1H NMR spectra confirmed the expected hydrogen proton distribution in the synthesized N-(3-(2-chloroacetoxy)propyl)-N,N-dimethyldodecan-1-aminium bromide.

3.1.3. N-(3-(2-(isopropyldimethylammonio)acetoxy)propyl)-N,N-dimethyldodecan-1-aminium chloride bromide (InhibitorQ1)

3.1.3.1. ^1H NMR spectroscopy. ^1H NMR (DMSO-d_6) spectrum (Fig. 4) of N-(3-(2-(isopropyldimethylammonio)acetoxy)propyl)-N,N-dimethyldodecan-1-aminium chloride bromide showed different bands at δ = 0.8411 ppm (t, 3H, $NCH_2CH_2(CH_2)_9C\underline{\mathbf{H}}_3$); δ = 1.2140 ppm (m, 18H, $NCH_2CH_2(C\underline{\mathbf{H}}_2)_9CH_3$); δ = 1.6879 ppm (m, 2H, $NCH_2C\underline{\mathbf{H}}_2(CH_2)_9CH_3$); δ = 3.3951 ppm (t, 2H, $NC\underline{\mathbf{H}}_2CH_2(CH_2)_9CH_3$); δ = 3.1964 ppm (s, 12H, $2(C\underline{\mathbf{H}}_3NC\underline{\mathbf{H}}_3)$); δ = 3.3080 ppm (t, 2H, $NC\underline{\mathbf{H}}_2CH_2CH_2COOCH_2N$); δ = 1.9890 ppm (t, 2H, $NCH_2C\underline{\mathbf{H}}_2CH_2COOCH_2N$); δ = 4.2312 ppm (t, 2H, $NCH_2CH_2C\underline{\mathbf{H}}_2COOCH_2N$); δ = 4.3107 ppm (s, 2H, $NCH_2CH_2CH_2COOC\underline{\mathbf{H}}_2N$); δ = 2.7287 ppm (m, 1H,$COONC\underline{\mathbf{H}}(CH_3)_2$; δ = 1.3547 ppm (d, 6H,$COONCH(C\underline{\mathbf{H}}_3)_2$. The data of ^1H NMR spectra confirmed the expected hydrogen proton distribution in the synthesized N-(3-(2-(isopropyldimethylammonio)acetoxy)propyl)-N,N-dimethyldodecan-1-aminium chloride bromide.

3.1.4. N-(3-(2-((2-hydroxyethyl)dimethylammonio)acetoxy)propyl)-N,N-dimethyldodecan-1-aminium chloride bromide (InhibitorQ2)

3.1.4.1. ^1H NMR spectroscopy. ^1H NMR (DMSO-d_6) spectrum (Fig. 5) of N-(3-(2-((2-hydroxyethyl)dimethylammonio)-acetoxy)propyl)-N,N-dimethyldodecan-1-aminium chloride bromide showed dif-

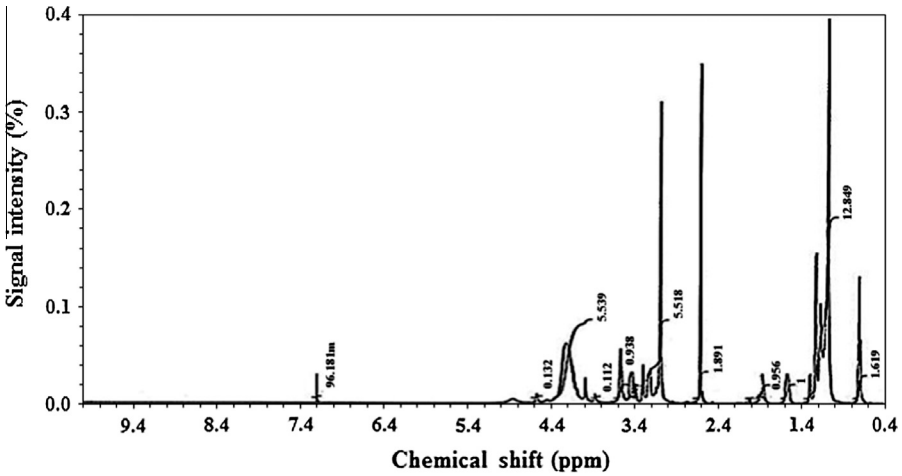

Fig. 4. ^1H NMR spectrum of N-(3-(2-(isopropyldimethylammonio)acetoxy)propyl)-N,N-dimethyldodecan-1-aminium chloride bromide.

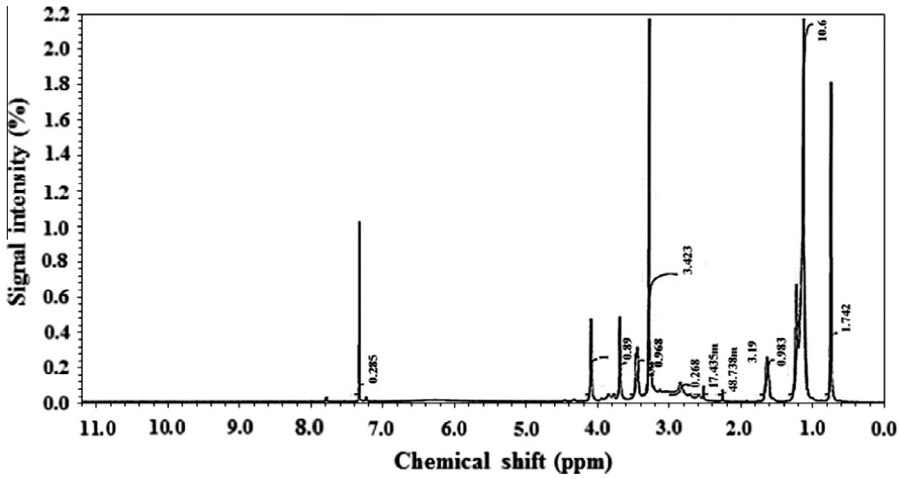

Fig. 5. ^{1}H NMR spectrum of N-(3-(2-((2-hydroxyethyl)dimethylammonio)acetoxy)propyl)-N,N-dimethyldodecan-1-aminium chloride bromide.

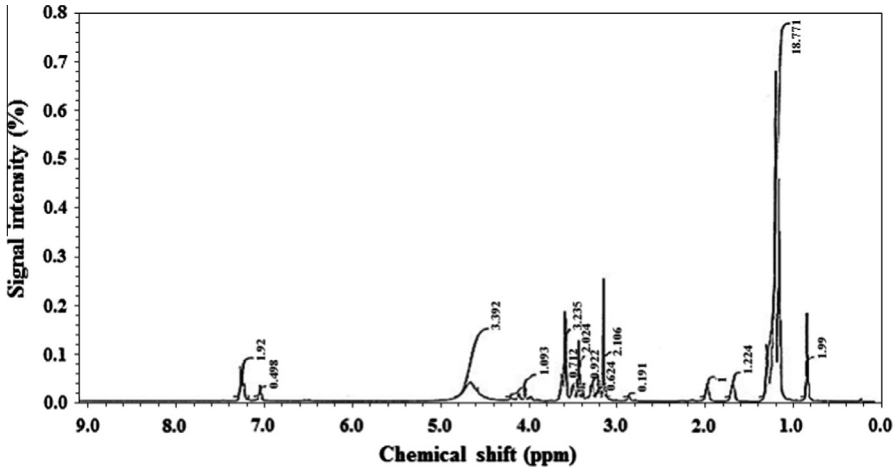

Fig. 6. ^{1}H NMR spectrum of N-(3-(2-(phenyldiethylammonio)acetoxy)propyl)-N,N-dimethyldodecan-1-aminium chloride bromide.

ferent bands at δ = 0.8671 ppm (t, 3H, $NCH_2CH_2(CH_2)_9C\underline{\mathbf{H}}_3$); δ = 1.2415 ppm (m, 18H, $NCH_2CH_2(C\underline{\mathbf{H}}_2)_9CH_3$); δ = 1.7291 ppm (m, 2H, $NCH_2C\underline{\mathbf{H}}_2(CH_2)_9CH_3$); δ = 3.4991 ppm (t, 2H, $NC\underline{\mathbf{H}}_2CH_2(CH_2)_9CH_3$); δ = 3.3401 ppm (s, 12H, $2(C\underline{\mathbf{H}}_3NC\underline{\mathbf{H}}_3)$); δ = 3.5159 ppm (t, 2H, $NC\underline{\mathbf{H}}_2CH_2CH_2COOCH_2N$); δ = 2.000 ppm (t, 2H, $NCH_2C\underline{\mathbf{H}}_2CH_2COOCH_2N$); δ = 4.1166 ppm (t, 2H, $NCH_2CH_2C\underline{\mathbf{H}}_2COOCH_2N$); δ = 4.1166 ppm (s, 2H, $NCH_2CH_2CH_2COOC\underline{\mathbf{H}}_2N$); δ = 3.5159 ppm (t, 2H, $NC\underline{\mathbf{H}}_2CH_2OH$); δ = 3.7268 ppm (t, 2H, $NCH_2C\underline{\mathbf{H}}_2OH$); δ = 7.2545 ppm (s, 1H, $NCH_2CH_2O\underline{\mathbf{H}}$). The data of ^{1}H NMR spectra confirmed the expected hydrogen proton distribution in the synthesized N-(3-(2-((2-hydroxyethyl)dimethylammonio)acetoxy)propyl)-N,N-dimethyldodecan-1-aminium chloride bromide.

3.1.5. N-(3-(2-(phenyldiethylammonio)acetoxy)propyl)-N,N-dimethyldodecan-1-aminium chloride bromide (Inhibitor Q3)

3.1.5.1. ^{1}H NMR spectroscopy. ^{1}H NMR (DMSO-d_6) spectrum (Fig. 6) of N-(3-(2-(phenyldiethylammonio)acetoxy)propyl)-N,N-dimethyldodecan-1-aminium chloride bromide showed different bands at δ = 0.7861 ppm (t, 3H, $NCH_2CH_2(CH_2)_9C\underline{\mathbf{H}}_3$); δ = 1.1132 ppm (m, 18H, $NCH_2CH_2(C\underline{\mathbf{H}}_2)_9CH_3$); δ = 1.6451 ppm (m, 2H, $NCH_2C\underline{\mathbf{H}}_2(CH_2)_9CH_3$); δ = 3.4165 ppm (t, 2H, $NC\underline{\mathbf{H}}_2CH_2(CH_2)_9CH_3$); δ = 3.1414 ppm (s, 12H, $2(C\underline{\mathbf{H}}_3NC\underline{\mathbf{H}}_3)$); δ = 3.5678 ppm (t, 2H, $NC\underline{\mathbf{H}}_2CH_2CH_2COOCH_2N$); δ = 1.9431 ppm (t, 2H, $NCH_2C\underline{\mathbf{H}}_2CH_2COOCH_2N$); δ = 4.5919 ppm (t, 2H, $NCH_2CH_2C\underline{\mathbf{H}}_2COOCH_2N$); δ = 4.6699 ppm (s, 2H, $NCH_2CH_2CH_2COOC\underline{\mathbf{H}}_2N$); δ = 3.5969 ppm (d, 6H,$COON(CH_2C\underline{\mathbf{H}}_3)_2$; δ = 1.1605 ppm (d, 6H,$COON(CH_2C\underline{\mathbf{H}}_3)_2$; δ = 7.3339 ppm (d, 2H, o-benzelidine nucleus); δ = 7.3339 ppm (t, 2H, m-benzelidine nucleus); δ = 7.1200 ppm (t, 1H, p-benzelidine nucleus). The data of ^{1}H NMR spectra confirmed the expected hydrogen proton distribution in the synthesized N-(3-(2-(phenyldiethylammonio)acetoxy)propyl)-N,N-dimethyldodecan-1-aminium chloride bromide.

3.2. Weight loss

The inhibition efficiency of the prepared cationic surfactants was determined in a test solution of 1 M HCl on API X65 steel pipeline surface. The value of corrosion rate (k) was calculated from the following equation [27]:

$$k = \frac{\Delta W}{St} \tag{1}$$

where ΔW is the average weight loss of three parallel API X65 steel pipeline sheets, S is the total area of the specimen, and t is the immersion time.

The surface coverage, θ, and the corrosion inhibition efficiency, (η_w), on API X65 steel pipelines were calculated using the following equations [28,29]:

$$\theta = \left(\frac{W - W_o}{W}\right) \tag{2}$$

$$\eta_w = \left(\frac{W - W_o}{W}\right) \times 100 \quad (3)$$

where W and W_o are the values of the weight loss without and with addition of the inhibitor, respectively.

Fig. 7 shows the behavior of API X65 steel pipeline in the presence of the inhibitor Q3 as a representative of the synthesized inhibitors at different concentrations and various temperatures. The corrosion rate, surface coverage and corrosion inhibition efficiency values of API X65 steel pipeline in 1 M HCl with and without different concentrations of the synthesized inhibitors at various temperatures are listed in Table 1. It was observed that the corrosion inhibition efficiency increased with increasing the concentration and decreasing the temperature. The best efficiency was obtained at 5×10^{-3} M at 20 °C. The inhibition efficiency of the studied inhibitors at different concentrations followed this order:

Q3 > Q2 > Q1

The obtained results were found to be in agreement with the general structure of the synthesized di-quaternary surfactants where the best efficiency obtained for surfactant (Q3) that has the highest electronic density located on the molecular head, which is composed of the benzene ring along with the ethanol and isopropyl groups. The head molecule is located coplanar to the metallic surface with the aliphatic chain placed perpendicular to the surface to retard the corrosive medium; these features facilitate the adsorption process on the metallic surface. Consequently, the increase of the inhibitor efficiency was ascribed to the molecular weight only, which is directly related to the head group of the synthesized di-quaternary ammonium salts and also to the surface extent coverage. In addition, molecules that were adsorbed on the metallic surface to form a more compact layer on it, which in turns reduced the diffusion of the corrosive medium towards the substrate. On the other hand, the film formed by the compound Q3 is more compact than that of Q2 and Q1 which is due to its higher electronic density located on the molecular head.

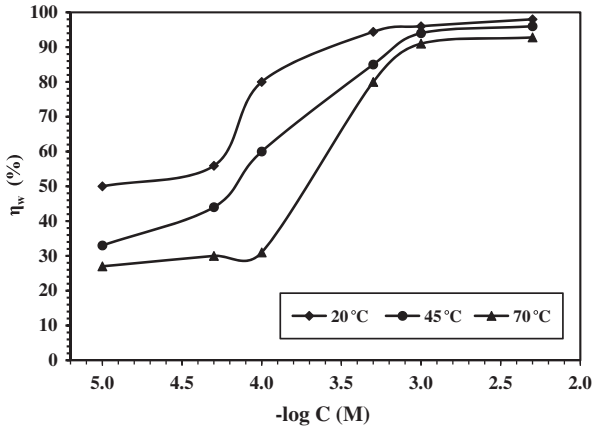

Fig. 7. Variation of the inhibition efficiency with different concentrations of inhibitor Q2 at various temperatures.

3.3. Electrochemical impedance measurements

In order to gain more information about the corrosion inhibition phenomena, EIS measurements was carried out for API X65 steel pipeline in 1 M HCl solution in the presence and absence of the synthesized di-quaternary ammonium salts. Fig. 8 shows Nyquist plots of the effect of the prepared surfactants concentration on the impedance response of API X65 steel pipeline in 1 M HCl solution at 20 °C. Inspection of the data revealed that the response of the system in the Nyquist complex plane is depressed semicircle which is attributed to the heterogeneity of the surface and the surface roughness [30].

Fig. 9 shows Bode plots of the effect of the prepared surfactants concentration on the impedance response of API X65 steel pipeline in 1 M HCl solution at 20 °C. As seen from Fig. 9, Bode plots refer to the existence of an equivalent circuit that contains a single constant phase element in the metal/solution interface. The increase of absolute impedance at low frequencies in Bode plot confirmed the higher protection with the increasing of inhibitor concentration, which is related to the adsorption of inhibitor on the carbon steel surface [31]. Fig. 10 shows Phase plots of the effect of the prepared surfactants concentration on the impedance response of API X65 steel pipeline in 1 M HCl solution at 20 °C. Fig. 10 shows one time constant only at all concentrations of the synthesized inhibitors. Also, it shows that the phase angle depression at relaxation frequency decreased with increasing the inhibitor concentration which indicated that the capacitive response increased with increasing the inhibitor concentration. This behavior could be

Table 1
Potentiodynamic polarization parameters for carbon steel corrosion in 1.0 M HCl in the absence and presence of different concentrations of the synthesized di-quaternary ammonium salts at 20 °C

Inhibitor name	Conc. of inhibitor (M)	E_{corr} mV(SCE)	i_{corr} (mA cm^{-2})	β_a (mV dec^{-1})	β_c (mV dec^{-1})	η_p (%)
Absence	0.00	−511	0.4837	166	−151	–
Q1	1×10^{-5}	−508	0.2861	153	−142	41.45
	5×10^{-5}	−513	0.2496	150	−197	48.40
	1×10^{-4}	−520	0.1421	148	−159	70.62
	5×10^{-4}	−526	0.0353	142	−143	92.70
	1×10^{-3}	−524	0.0253	143	−165	94.77
	5×10^{-3}	−527	0.0221	142	−143	95.43
Q2	1×10^{-5}	−513	0.2514	170	−191	49.62
	5×10^{-5}	−509	0.1942	176	−156	59.85
	1×10^{-4}	−507	0.1151	129	−194	76.20
	5×10^{-4}	−515	0.0294	145	−148	93.92
	1×10^{-3}	−508	0.0226	189	−171	95.33
	5×10^{-3}	−505	0.0182	149	−178	96.24
Q3	1×10^{-5}	−512	0.2176	168	−150	55.01
	5×10^{-5}	−506	0.1087	125	−169	77.53
	1×10^{-4}	−520	0.0857	163	−150	82.28
	5×10^{-4}	−423	0.0287	117	−149	94.07
	1×10^{-3}	−526	0.0163	188	−188	96.63
	5×10^{-3}	−525	0.0136	189	−188	97.19

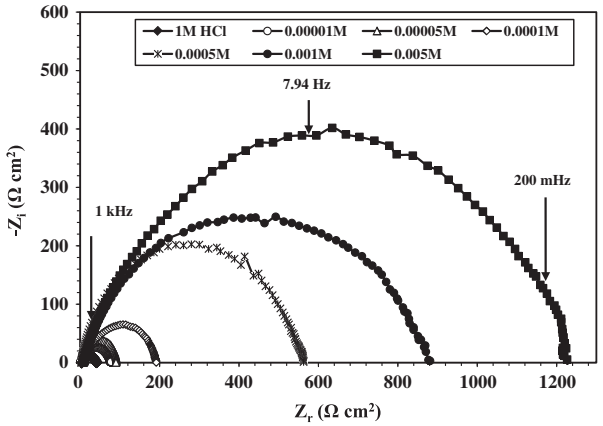

Fig. 8. Nyquist plots for API X65 steel pipeline in 1 M HCl in absence and presence of different concentrations of inhibitor Q2.

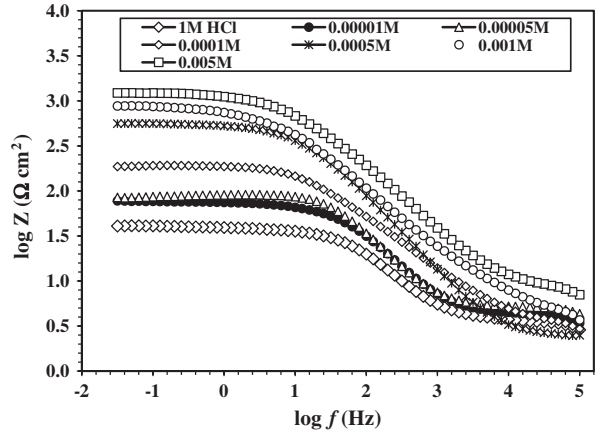

Fig. 9. Bode plots for API X65 steel pipeline in 1 M HCl in the absence and presence of different concentrations of inhibitor Q2.

attributed to the corrosion activity which is decreased with increasing the concentration of the synthesized inhibitors.

From EIS results, an electrical equivalent circuit (EEC) could be proposed to model the electrolyte/steel interface, presented in Fig. 11. This EEC is constituted of one constant phase elements, respectively, composed of a component Y_o and a coefficient n. The coefficient n can characterize different physical phenomena like surface inhomogeneous resulting from surface roughness, impurities, inhibitor adsorption and porous layer formation.

The impedance, Z_{CPE}, for a circuit including a CPE was calculated from the following equation [32,33]:

$$Z_{CPE} = \frac{1}{Y_o(J\omega)^n} \tag{4}$$

where Y_o is a proportional factor, $J^2 = -1$, $\omega = 2\pi f$ and n is the phase shift. For $n = 0$, Z_{CPE} represents a resistance with $R = Y_o^{-1}$, for $n = 1$ a capacitance with $C = Y_o$, for $n = 0.5$ a Warburg impedance with $W = Y_o$ and for $n = -1$ an inductive with $L = Y_o^{-1}$.

The double layer capacitance, C_{dl}, for a circuit including a CPE was calculated from the following equation [32,33]:

$$C_{dl} = Y_o(\omega_{max})^{n-1} \tag{5}$$

where $\omega_{max} = 2\pi f_{max}$ and f_{max} is the frequency at which the imaginary component of the impedance is maximal.

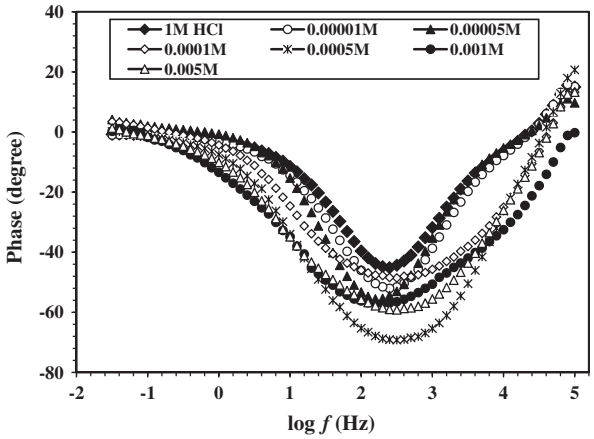

Fig. 10. Phase angle plots for API X65 steel pipeline in 1 M HCl solution in the absence and presence of different concentrations of inhibitor Q2.

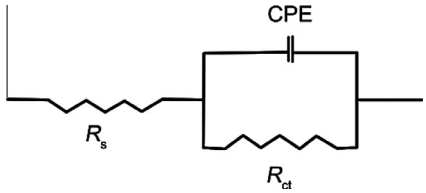

Fig. 11. Suggested equivalent circuit model for the studied systems.

The inhibition efficiency (η_I) was calculated using the following equation [34]:

$$\eta_I = \left(\frac{R_{ct}^o - R_{ct}}{R_{ct}^o}\right) \times 100 \tag{6}$$

where R_{ct}^o and R_{ct} are the charge transfer resistance values in the presence and absence of the inhibitor, respectively.

Solution resistance (R_s), charge transfer resistance (R_{ct}) and double layer capacitance (C_{dl}) were determined using EIS measurements and given in Table 2. These parameters could be concluded as follows:

(1) The diameter of Nyquist semicircle (charge transfer resistance (R_{ct})) increased with increasing the concentration of the synthesized di-quaternary ammonium salts indicating that the corrosion resistance of the API X65 steel pipeline samples is mainly controlled by charge-transfer process.
(2) C_{dl} values decreased with increasing inhibitor concentration. This is due to the gradual replacement of water molecules in the double layer by the adsorbed inhibitor molecules which form on adherent film on the metal surface and lead to decrease in the local dielectric constant of the metal solution interface.
(3) The inhibition efficiency of three synthesized inhibitors increased with increasing inhibitor concentration. This is due to increasing the surface coverage by the inhibitor.
(4) The corrosion inhibition efficiency of three synthesized inhibitors decreased in the following sequences: Q3 > Q2 > Q1.

3.4. Polarization measurements

Potentiodynamic polarization curves for API X65 steel pipeline in 1.0 M HCl containing various concentrations of inhibitor Q3 at 20 °C are shown in Fig. 12. The corrosion current density values

were estimated accurately by extrapolating both the cathodic and anodic linear region back to the corrosion potential.

The inhibition efficiency (η_p) was calculated using the following equation [23]:

$$\eta_p = \left(\frac{i_{corr} - i^o_{corr}}{i_{corr}}\right) \times 100 \quad (7)$$

where i^o_{corr} and i_{corr} are the corrosion current density values with and without inhibitor, respectively.

The electrochemical corrosion parameters of corrosion current densities (i_{corr}), corrosion potential (E_{corr}), cathodic Tafel slope (β_c), anodic Tafel slope (β_a) and the inhibition efficiency (η_p) as functions of inhibitors concentrations, are given in Table 3. These parameters could be concluded as follows:

(1) The corrosion current density (i_{corr}) decreased with increasing the concentration of the three synthesized inhibitors which indicated that these compounds act as inhibitors, and the degree of inhibition depends on the concentrations of inhibitor.
(2) The presence of the synthesized di-quaternary ammonium salts are slightly shifted E_{corr} to negative and positive direction, which indicates that the synthesized di-quaternary ammonium salts act as a mixed-type inhibitor [35].
(3) Tafel slope of β_c and β_a is slightly changed upon addition of inhibitors compared to blank, which implies that the inhibitors molecules are blocked for both cathodic and anodic sites resulting in an inhibition of the cathodic and anodic reactions.
(4) The corrosion inhibition efficiency of three synthesized inhibitors decreases in the following sequences Q3 > Q2 > Q1.

It could be concluded that the inhibition efficiency found from weight loss, electrochemical impedance spectroscopy and polarization curves measurements are in a good agreement.

3.5. Adsorption isotherm

The adsorption of inhibitor molecules on metal surface is a substitute process, in which the water molecules adsorbed on the metal surface are replaced by inhibitor molecules. In order to get a better understanding for the adsorption mechanism, the Langmuir adsorption isotherm equation was employed [36]:

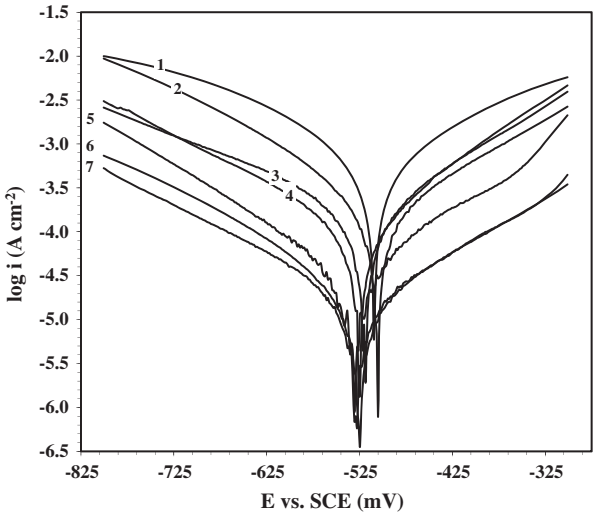

Fig. 12. Anodic and cathodic polarization curves for API X65 steel pipeline obtained at 20 °C in 1 M HCl solution in the absence and presence of different concentrations of inhibitor Q2. (1) 1 M HCl, (2) 1×10^{-5} M, (3) 5×10^{-5} M, (4) 1×10^{-4} M, (5) 5×10^{-4} M, (6) 1×10^{-3} M and (7) 5×10^{-3} M.

$$\frac{C}{\theta} = \frac{1}{K_{ads}} + C \quad (8)$$

where θ is the surface coverage, which can be calculated from the weight loss experimental results, C is the molar concentration of the inhibitor and K_{ads} is the standard adsorption equilibrium constant.

The plots of C/θ versus C yielded a straight line with a slope near 1 at different temperatures as shown in Fig. 13. This isotherm clearly revealed that the adsorption of the synthesized di-quaternary ammonium salts on the API X65 steel pipeline surface obeyed the Langmuir adsorption isotherm and the inhibitor molecules are adsorbed on API X65 steel pipeline surface forming a film, which prevents the API X65 steel pipeline from corrosion induced by the medium. The standard adsorption equilibrium constant (K_{ads}) of the synthesized di-quaternary ammonium salts are given in Table 4. It can be seen that K_{ads} values decreased with temperature

Table 2
EIS parameters for corrosion of carbon steel in 1.0 M HCl in the absence and presence of different concentrations of the synthesized di-quaternary ammonium salts at 20 °C

Inhibitor name	Conc. of inhibitor (M)	R_s (Ω cm^2)	Q_{dl} (Ω^{-1} s^n cm^{-2})	n	Error of n	R_{ct} (Ω cm^2)	C_{dl} (μF cm^{-2})	η_I (%)
Absence	0.00	3.52	0.0002215	0.83	1.22	36.2	128.2	–
Q1	1×10^{-5}	1.24	0.0001798	0.90	2.24	57.5	80.6	37.0
	5×10^{-5}	1.25	0.0001745	0.90	1.94	66.7	71.8	45.7
	1×10^{-4}	2.80	0.0001585	0.79	0.93	133.1	35.5	72.8
	5×10^{-4}	3.67	0.0001366	0.71	0.68	457.7	19.5	92.1
	1×10^{-3}	3.26	0.0000656	0.81	0.56	550.7	11.1	93.4
	5×10^{-3}	3.04	0.0000210	0.86	0.59	1079.0	9.0	96.6
Q2	1×10^{-5}	4.19	0.0001263	0.85	1.04	70.85	69.8	48.9
	5×10^{-5}	5.11	0.0000803	0.91	0.79	85.0	51.3	57.4
	1×10^{-4}	3.46	0.0000751	0.71	1.05	193.2	27.0	81.2
	5×10^{-4}	2.66	0.0000598	0.86	1.02	541.0	15.5	93.3
	1×10^{-3}	4.28	0.0000429	0.70	0.50	870.5	9.6	95.8
	5×10^{-3}	8.34	0.0000391	0.76	0.75	1203.0	6.3	97.0
Q3	1×10^{-5}	1.82	0.0000129	0.91	1.22	78.3	70.5	53.7
	5×10^{-5}	2.03	0.0000513	0.85	1.04	174.7	24.7	79.3
	1×10^{-4}	3.09	0.0000437	0.64	1.12	248.0	22.9	85.4
	5×10^{-4}	2.95	0.0000359	0.80	0.83	921.7	10.5	96.1
	1×10^{-3}	3.28	0.0000246	0.70	0.50	1479.0	6.9	97.6
	5×10^{-3}	3.71	0.0000110	0.70	0.50	1566.0	4.6	97.7

Table 3
Weight loss data for carbon steel 1.0 M HCl in the absence and presence of different concentrations of the synthesized di-quaternary ammonium salts at various temperatures

Inhibitor name	Inhibitor conc. (M)	20 °C			45 °C			70 °C		
		k (mg cm^{-2} h^{-1})	θ	η_w (%)	k (mg cm^{-2} h^{-1})	θ	η_w (%)	k (mg cm^{-2} h^{-1})	θ	η_w (%)
Absence	0.00	0.463	–	–	2.372	–	–	8.319	–	–
Q1	1×10^{-5}	0.277	0.40	40.0	1.660	0.30	30.0	6.110	0.27	26.5
	5×10^{-5}	0.240	0.50	50.0	1.510	0.39	39.2	6.010	0.29	28.5
	1×10^{-4}	0.150	0.73	73.0	1.410	0.50	50.0	5.990	0.30	30.0
	5×10^{-4}	0.035	0.92	92.0	0.360	0.84	84.0	1.650	0.79	79.0
	1×10^{-3}	0.011	0.94	94.0	0.113	0.92	92.0	0.595	0.90	90.0
	5×10^{-3}	0.009	0.97	97.0	0.099	0.95	94.5	0.511	0.91	91.0
Q2	1×10^{-5}	0.250	0.50	50.0	1.610	0.33	33.0	6.080	0.28	27.5
	5×10^{-5}	0.204	0.60	55.9	1.420	0.44	44.0	5.950	0.30	30.0
	1×10^{-4}	0.111	0.80	80.0	1.190	0.60	60.0	5.900	0.31	31.0
	5×10^{-4}	0.029	0.94	94.4	0.333	0.85	85.0	1.590	0.81	80.6
	1×10^{-3}	0.009	0.96	96.0	0.099	0.94	94.0	0.510	0.91	91.0
	5×10^{-3}	0.007	0.98	98.0	0.091	0.96	96.0	0.501	0.93	92.8
Q3	1×10^{-5}	0.208	0.55	55.0	1.542	0.35	35.0	5.990	0.29	28.5
	5×10^{-5}	0.110	0.79	79.0	1.300	0.49	49.0	5.710	0.32	32.0
	1×10^{-4}	0.092	0.86	85.5	0.995	0.63	62.5	5.600	0.35	35.0
	5×10^{-4}	0.022	0.96	95.5	0.307	0.86	86.2	1.510	0.82	82.0
	1×10^{-3}	0.006	0.99	98.5	0.083	0.97	96.5	0.416	0.95	95.0
	5×10^{-3}	0.003	1.0	99.5	0.059	0.98	97.5	0.322	0.96	96.0

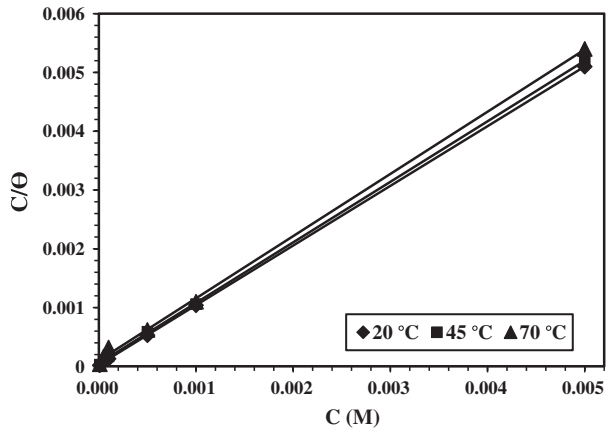

Fig. 13. Langmuir's adsorption plots for API X65 steel pipeline in 1 M HCl solution containing different concentrations of inhibitor Q2 at 20 °C.

Table 4
Standard thermodynamic parameters of the adsorption on carbon steel surface in 1.0 M HCl containing different concentrations of the synthesized di-quaternary ammonium salts at various temperatures

Inhibitor name	Temperature (°C)	K_{ads} ($\times 10^4$ M^{-1})	ΔG^o_{ads} kJ mol^{-1}	ΔH^o_{ads} kJ mol^{-1}	ΔJ^o_{ads} J mol^{-1} K^{-1}
Q1	20	3.33	−35.15	−20.76	49.11
	45	1.63	−36.26		48.74
	70	0.98	−37.66		49.27
Q2	20	3.99	−35.6	−22.97	43.10
	45	1.98	−36.78		43.42
	70	1.00	−37.72		43.00
Q3	20	6.61	−36.82	−30.13	22.83
	45	2.17	−37.02		21.67
	70	1.08	−37.94		22.77

increasing, suggesting that the elevated temperature facilitates the desorption of the synthesized inhibitors from API X65 steel pipeline surface and hence, the adsorption of the inhibitor decreased with the increasing of temperature. The high value of K_{ads} indicated that the synthesized inhibitors possess strong adsorption ability onto the API X65 steel pipeline surface.

The standard free energy of adsorption (ΔG^o_{ads}) was calculated by the following equation [37]:

$$\Delta G^o_{ads} = -RT \ln(55.5 K_{ads}) \quad (9)$$

where the value of 55.5 is the molar concentration of water in the solution expressed in molarity unit, R is the universal gas constant and T is the absolute temperature.

The standard free energy of adsorption (ΔG^o_{ads}) of the synthesized di-quaternary ammonium salts are given in Table 4. It can be seen that all ΔG^o_{ads} values for the synthesized inhibitors are ranged between −20 and −40 kJ mol^{-1} which indicated that the adsorption mechanism of the prepared di-quaternary ammonium salts on the API X65 steel pipeline surface in 1 M HCl solution is a mixed from physical and chemical adsorption [38].

The enthalpy can be deduced from the Van't Hoff equation [39–42].

$$\ln K_{ads} = -\left(\frac{\Delta H^o_{ads}}{RT}\right) + \text{constant} \quad (10)$$

where K_{ads} is the standard adsorption equilibrium constant, ΔH^o_{ads} is the adsorption heat, which can be determined from the slope ($-\Delta H^o_{ads}/R$) of the line ln K_{ads} against $1/T$ (see Fig. 14). The standard adsorption enthalpy values obtained from Eq. (9) are also given in Table 4. The obtained negative values of ΔH_{ads} confirm the exothermic behavior of the adsorption process of the prepared di-quaternary ammonium salts on the API X65 steel pipeline surface in 1 M HCl solution. While, an endothermic adsorption process ($\Delta H_{ads} > 0$) is attributed unequivocally to chemisorption. An exothermic adsorption process ($\Delta H_{ads} < 0$) may involve either physisorption or chemisorption or a mixture of both processes [43,44].

The standard adsorption entropy, ΔS^o_{ads}, was calculated from the following equation [45,46]:

$$\Delta G^o_{ads} = \Delta H^o_{ads} - T\Delta S^o_{ads} \quad (11)$$

The standard adsorption entropy values obtained from Eq. (11) are also given in Table 4. Inspection of Table 4 revealed that the sign of ΔS^o_{ads} is positive. This is opposite to what would be expected, since adsorption is always accompanied by a decrease of entropy. The reason could be explained as follow: The adsorption of organic inhibitor molecules from the aqueous solution can be regarded as a quasi-substitution process between the organic compound in

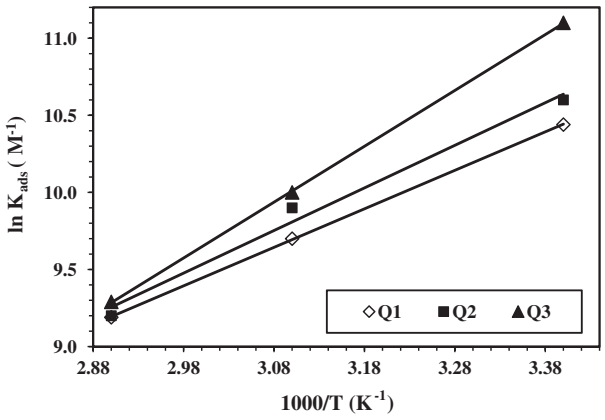

Fig. 14. The relationship between ln K_{ads} and $1/T$ for API X65 steel pipeline in 1 M HCl solution containing different concentrations of the synthesized novel di-quaternary ammonium salts.

the aqueous phase [$Org_{(sol)}$] and water molecules at the electrode surface [$H_2O_{(ads)}$]

$$Org_{(sol)} + xH_2O_{(ads)} \leftrightarrow Org_{(ads)} + xH_2O_{(sol)} \quad (12)$$

where x is the size ratio, which is the number of water molecules replaced by one organic inhibitor. In this situation, the adsorption of the synthesized di-quaternary ammonium salts is accompanied by desorption of water molecules from the surface. Thus, when the adsorption process for the inhibitor is believed to be associated with a decrease in entropy of the solute, the opposite is true for the solvent. The thermodynamic values obtained are the algebraic sum of the adsorption of organic molecules and desorption of water molecules [47]. Therefore, the gain in entropy is attributed to the increase in solvent entropy. The positive values of ΔS^{o}_{ads} also mean that an increasing in disordering takes place in reactants adsorption form inhibitor to the metal/solution interface, which is the driving force for the adsorption of inhibitor onto steel surface [48].

3.6. Inhibition mechanism

The adsorption of organic molecules on the solid surfaces may be physisorption or chemisorption or a mixture of both processes. In physical adsorption, inhibitor molecules can also be adsorbed on the steel surface via electrostatic interaction between the charged metal surface and the charged inhibitor molecule. Chemical adsorption of the inhibitors arises from the donor acceptor interactions between the free electron pairs of heteroatoms and π-electrons of multiple bonds as well as a phenyl group and vacant d-orbital's of iron [49,50]. The orientation of molecules may depend on the pH and/or electrode potential [51]. In the case of parallel adsorption of inhibitor molecules, the steric factors also must be taken into consideration. The adsorption free energy values are ranged between −20 and −40 kJ mol^{-1} which indicate that the adsorption mechanism of the prepared di-quaternary ammonium salts on the API X65 steel pipeline surface in 1 M HCl solution is a mixed of physical and chemical adsorption.

Because API X65 steel pipeline surface has a positive charge, Cl^- ions may be adsorbed first onto the positively charged metal surface, and then the inhibitor molecules are adsorbed through electrostatic interactions between the negatively charged metal surface and positively charged di-quaternary ammonium salts molecules (Q^+) and form a protective $(FeCl^-Q^+)_{ads}$ layer. Cationic surfactant molecules are also adsorbed at cathodic sites of metal in competition with hydrogen ions, while counters ions are adsorbed on the anodic sites of metal or formed $(FeCl^-Q^+Br^-)_{ads}$ layer to retard the dissolution of metals. At high temperatures, the donor acceptor interaction between free electron pairs of nitrogen and oxygen atoms of the synthesized inhibitors and vacant d-orbital's of iron was found. The adsorption of cationic surfactant molecules reduced the rate of hydrogen evolution reaction. Finally, the high inhibition efficiency of the synthesized di-quaternary ammonium salts can be contributed to the presence of two ammonium ions as polar groups and one fatty alkyl chain as a nonpolar group. Therefore, its concentration at the interface is larger than in the bulk of corrosive media. In addition, a large size and a high molecular weight of the synthesized di-quaternary ammonium salts molecules can also contribute to the greater inhibition efficiency. It was found that the best di-quaternary ammonium salts was inhibitor (Q3). This could be due to benzene ring (more activating) existing in inhibitor (Q3), which can form coordinated bonds with X65 steel pipeline through the presence of three double bonds and lone pairs of electrons, in addition to the hydrophobicity and planarity of benzene ring on the steel surface. However, (–OH) group is weaker electron donors (moderately activating) than a benzene ring and hence inhibitor (Q2) showed a lower inhibition efficiency than inhibitor (Q3). Likewise, isopropyl group ($-CH(CH_3)_2$) group is not an electron donor (not activating) and hence, inhibitor (Q1) showed the lowest inhibition efficiency. Therefore, inhibitor (Q3) has more binding molecules with the metal and thereby more inhibition efficiency was observed.

The prepared surfactants showed more enhanced inhibition efficiency values than the reported ones [52–55]. It was reported recently that the inhibition efficiency of mild steel corrosion in HCl solution by triazole derivatives, 5-amino-1,2,4-triazole, 5-amino-3-mercapto-1,2,4-triazole, 5-amino-3-methylthio-1,2,4-triazole and 1-amino-3-methylthio-1,2,4-triazole reached 65–84% at 1×10^{-2} M [52]. Also, it was found that benzimidazole, 2-hydroxybenzimidazole, 2-aminomethylbenzimidazole, 2-(2-pyridyl)benzimidazole and 2-aminobenzimidazole exhibited inhibition efficiency percentages, 51.0–78.2%, using amounts of the inhibitors in the range of 1×10^{-2} M [53]. In the same respect, Khaled et al. [54] reported that the inhibition efficiency of mild steel corrosion in HCl solution by 4-methyl pyrazole reached only 70.13% at 1×10^{-2} M and duplication of the added amount achieved efficiency of 97.7%. In addition, Amin et al. [55] have studied the applicability of alanine, cysteine and S-methyl cysteine as corrosion inhibitors for iron in 1 M HCl and showed that the inhibition efficiency for these compounds reached 75.0–92.9% in the presence of concentration equals 5×10^{-3} M.

The adsorption of inhibitor molecules depends mainly on certain physicochemical properties such as the chemical nature of the functional groups, steric factors, aromaticity, electron density of the donor atoms, the p orbital character of the donating electrons and the electronic structure of the molecules. The superior inhibition efficiency of the prepared di-quaternary ammonium salts may be due to the fact that the surfactants are concentrated at the interface between carbon steel and corrosive solution more than the bulk which is opposite in the case of organic amines where their concentrations at interface and bulk of corrosive solution are approximately the same. The high performance of the investigated di-quaternary ammonium salt is attributed to the presence of many adsorption centers, large molecular size and the planarity of the compounds which covers wide areas of the metal surface and thus preventing the general corrosion.

4. Conclusions

(1) The synthesized novel di-quaternary ammonium salts inhibitors are good inhibitors for the corrosion of API X65 steel pipeline in 1 M HCl solution.

(2) Inhibition efficiency values increased with increasing the inhibitor concentration and decreasing the temperature. The inhibition efficiency increased in the order: Q3 > Q2 > Q1.
(3) The inhibitors acted as mixed-type inhibitors and the inhibition is caused by active sites blocking effect.
(4) EIS spectra exhibited one capacitive loop which indicated that the corrosion reaction is controlled by charge transfer process. The addition of inhibitors to 1 M HCl solution enhanced R_{ct} values while reduced C_{dl} values.
(5) The adsorption of inhibitors on API X65 steel pipeline surface obeyed Langmuir adsorption isotherm. The adsorption process is physically and exothermically which accompanied by an increase in the entropy.

References

[1] S. Ghareba, S. Omanovic, Corros. Sci. 52 (2010) 2104–2113.
[2] A. Hernández-Espejel, M.A. Domínguez-Crespo, R. Cabrera-Sierra, C. Rodríguez-Meneses, E.M. Arce-Estrada, E.M. Arce-Estrada, Corros. Sci. 52 (2010) 2258–2267.
[3] M.A. Hegazy, H.M. Ahmed, A.S. El-Tabei, Corros. Sci. 53 (2011) 671–678.
[4] E. Sadeghi Meresht, T. Shahrabi Farahani, J. Neshati, Eng. Failure Anal. 18 (2011) 963–970.
[5] O.K. Abiola, Corros. Sci. 48 (2006) 3078–3090.
[6] J.Z. Ali, X.P. Guo, J.E. Qu, Z.Y. Chen, J.S. Zheng, Colloids Surf. A: PhysicoChem. Eng. Aspects 281 (2006) 147–155.
[7] I. Dehri, M. Ozcan, Mater. Chem. Phys. 98 (2006) 316–323.
[8] L. Tang, X. Li, Li Lin, G. Mu, G. Liu, Mater. Chem. Phys. 97 (2006) 301–307.
[9] M.M.A. El-Sukkary, E.A. Soliman, D.A. Ismail, S.M. El Rayes, M.A. Saad, J. Tenside Surf. Det. 48 (2011) 82–86.
[10] S. Ramesh, S. Rajeswari, Electrochim. Acta 49 (2004) 811–820.
[11] A. Popova, E. Sokolova, S. Raicheva, M. Christov, Corros. Sci. 45 (2003) 33–58.
[12] R. Solmaz, G. Kardas, B. Yazıcı, M. Erbil, Colloids Surf. A: PhysicoChem. Eng. Aspects 312 (2008) 7–17.
[13] F. Bentiss, F. Gassama, D. Barbry, L. Gengembre, H. Vezin, M. Lagrenée, M. Traisnel, Appl. Surf. Sci. 252 (2006) 2684–2691.
[14] A. Ouchrif, M. Zegmout, B. Hammouti, A. Dafali, M. Benkaddour, A. Ramdani, S. Elkadiri, Prog. Org. Coat. 53 (2005) 292–296.
[15] L.J. Berchmans, V. Sivan, S.V.K. Iyer, Mater. Chem. Phys. 98 (2006) 395–400.
[16] G. Bereket, C. Ogretir, A. Yurt, J. Mol. Struct. (Theochem.) 571 (2001) 139–145.
[17] N. Khalid, Electrochim. Acta 48 (2003) 2635–2640.
[18] E. Stipnisek-Lisac, A. Gazivoda, M. Madzarac, Electrochim. Acta 47 (2002) 4189–4194.
[19] M. Sahin, S. Bilgic, H. Yilmaz, Appl. Surf. Sci. 195 (2002) 1–7.
[20] M.A. Hegazy, A.S. El-Tabei, J. Surf. Deter. 16 (2013) 221–232.
[21] D. Asefi, M. Arami, N.M. Mahmoodi, Corros. Sci. 52 (2010) 794–800.
[22] M.A. Hegazy, Corros. Sci. 51 (2009) 2610–2618.
[23] A.M. Badawi, M.A. Hegazy, A.A. El-Sawy, H.M. Ahmed, W.M. Kamel, Mater. Chem. Phys. 124 (2010) 458–465.
[24] M.A. Hegazy, M.F. Zaky, Corros. Sci. 52 (2010) 1333–1341.
[25] Hassan A. Shehata, Abd Allah Abd El-wahab, A. Hafiz, I. Aiad, M.A. Hegazy, J. Surf. Detr. 11 (2008) 139–144.
[26] S. Liu, N. Xu, J. Duan, Z. Zeng, Z. Feng, R. Xiao, Corros. Sci. 51 (2009) 1356–1363.
[27] I.L. Rosenfeld, Corrosion Inhibitors, McGraw-Hill, New York, 1981.
[28] R.A. Prabhu, T.V. Venkatesha, A.V. Shanbhag, G.M. Kulkarni, R.G. Kalkhambkar, Corros. Sci. 50 (2008) 3356–3362.
[29] K. Bhrara, H. Kim, G. Singh, Corros. Sci. 50 (2008) 2747–2754.
[30] M. Lebrini, M. Lagrenee, H. Vezin, M. Traisnel, F. Bentiss, Corros. Sci. 49 (2007) 2254–2269.
[31] M.A. Hegazy, Ali M. Hasan, M.M. Emara, Mostafa F. Bakr, Ahmed H. Youssef, Corros. Sci. 65 (2012) 67–76.
[32] Z.B. Stoynov, B.M. Grafov, B. Savova-Stoynova, V.V. Elkin, Electrochemical Impedance, Nauka, Moscow, 1991.
[33] A. Popova, M. Christov, A. Vasilev, Corros. Sci. 53 (2011) 1770–1777.
[34] A.M. Atta, O.E. El-Azabawy, H.S. Ismail, M.A. Hegazy, Corros. Sci. 52 (2011) 1680–1689.
[35] C. Cao, Corros. Sci. 38 (1996) 2073–2082.
[36] A. Doner, R. Solmaz, M. Ozcan, G. Kardas, Corros. Sci. 53 (2011) 2902–2913.
[37] G.E. Badr, Corros. Sci. 51 (2009) 2529–2536.
[38] M. Behpour, S.M. Ghoreishi, N. Soltani, M. Salavati-Niasari, M. Hamadanian, A. Gandomi, Corros. Sci. 50 (2008) 2172.
[39] X. Li, S. Deng, H. Fu, Corros. Sci. 53 (2011) 664–670.
[40] X.H. Li, S.D. Deng, G.N. Mu, H. Fu, F.Z. Yang, Corros. Sci. 50 (2008) 420–430.
[41] X.H. Li, S.D. Deng, H. Fu, Corros. Sci. 51 (2009) 1344–1355.
[42] X.H. Li, S.D. Deng, H. Fu, G.N. Mu, Corros. Sci. 50 (2008) 2635–2645.
[43] W. Durnie, R.D. Marco, A. Jefferson, B. Kinsella, J. Electrochem. Soc. 146 (1999) 1751–1756.
[44] S.A. Ali, A.M. El-Shareef, R.F. Al-Ghamdi, M.T. Saeed, Corros. Sci. 47 (2005) 2659–2678.
[45] H.A. Sorkhabi, B. Shaabani, D. Seifzadeh, Appl. Surf. Sci. 239 (2005) 154–164.
[46] M.A. Hegazy, M. Abdallah, H. Ahmed, Corros. Sci. 52 (2010) 2897–2904.
[47] V. Branzoi, F. Branzoi, M. Baibarac, Mater. Chem. Phys. 65 (2000) 288–297.
[48] X.H. Li, S.D. Deng, H. Fu, T.H. Li, Electrochim. Acta 54 (2009) 4089–4098.
[49] M. Behpour, S.M. Ghoreishi, M. Salavati-Niasari, B. Ebrahimi, Mater. Chem. Phys. 107 (2008) 153–157.
[50] A. Yurt, A. Balaban, S. UstunKandemir, G. Bereket, B. Erk, Mater. Chem. Phys. 85 (2004) 420–426.
[51] L. Vracar, D.M. Drazic, Corros. Sci. 44 (2002) 1669–1680.
[52] H.H. Hassan, E. Abdelghani, M.A. Amin, Electrochim. Acta 52 (2007) 6359–6366.
[53] K.F. Khaled, Electrochim. Acta 48 (2003) 2493–2503.
[54] K.F. Khaled, S.S. Abdel-Rehim, G.B. Sakr, Arab. J. Chem. 5 (2012) 213–218.
[55] M.A. Amin, K.F. Khaled, Q. Mohsen, H.A. Arida, Corros. Sci. 52 (2010) 1684–1695.